Astronomy & Astrophysics manuscript no. spectrum
October 23, 2007

Cumulative hard X-ray spectrum of local AGN: a link to the cosmic X-ray background

S. Sazonov[1,2], R. Krivonos[2,1], M. Revnivtsev[1,2], E. Churazov[1,2], and R. Sunyaev[1,2]

[1] Max-Planck-Institut für Astrophysik, Karl-Schwarzschild-Str. 1, D-85740 Garching bei München, Germany
[2] Space Research Institute, Russian Academy of Sciences, Profsoyuznaya 84/32, 117997 Moscow, Russia

Received / Accepted

ABSTRACT

Aims. We determine the cumulative spectral energy distribution of local AGN in the range 3–300 keV and compare it with the spectrum of the cosmic X-ray background (CXB) in order to test the widely accepted paradigm that the CXB is a superposition of active galactic nuclei (AGN) and to place constraints on AGN evolution.
Methods. We perform a stacking analysis of the hard X-ray spectra of AGN detected in two recent all-sky surveys, performed by the IBIS/ISGRI instrument aboard INTEGRAL and by the PCA instrument aboard RXTE, properly taking into account the space densities of AGN with different luminosities and absorption column densities.
Results. We derive the spectral energy distribution of the collective emission of local AGN in the 3–300 keV energy band. AGN with luminosities below $10^{43.5}$ erg s^{-1} (17–60 keV) provide the main contribution to the local volume emissivity in hard X-rays, at least 5 times as much as more luminous objects. The cumulative spectrum exhibits (although with marginal significance) a high-energy cutoff at energies above ∼100–200 keV and is consistent with the CXB spectrum if AGN evolve with cosmic time in such a way that their collective high-energy emission has a constant spectral shape and the relative fraction of obscured AGN does not change, while the AGN luminosity density undergoes strong evolution between $z \sim 1$ and $z = 0$, a scenario broadly consistent with results obtained from deep X-ray surveys.
Conclusions. The first direct comparison between the spectral energy distribution of the collective hard X-ray emission of local AGN and the CXB spectrum has demonstrated that the popular concept of the CXB being a superposition of AGN is grossly correct. By repeating this test using better AGN statistics coming from current and future hard X-ray telescopes it should be possible to tighten the constraints on the cosmic history of black hole growth.

Key words. Surveys – Galaxies: active – Galaxies: evolution – Galaxies: Seyfert – X-rays: diffuse background

1. Introduction

It is widely believed that the bulk of the cosmic X-ray background (CXB) consists of emission from all active galactic nuclei (AGN) in the visible Universe (Setti & Woltjer 1989). Therefore, the CXB represents a unique integral record of the history of growth of massive black holes since the early epochs till the present time. The popularity of this concept rests on the absence of significant distortions in the thermal spectrum of the cosmic microwave background, which rules out that a hot intergalactic medium is a major contributor to the CXB (Wright et al. 1994), and also on the fact that most of the CXB at energies below several keV has been directly resolved into individual AGN (see Brandt & Hasinger 2005 for a recent review).

However, the peak of the CXB spectral energy distribution is situated near 30 keV (e.g. Gruber et al. 1999), where ∼ 99% of the background emission remains unresolved (Krivonos et al. 2007). For this reason, currently popular CXB synthesis models (e.g. Gilli et al. 2007) confront versatile AGN statistics (source counts, luminosity functions at different redshifts, distribution of absorption column densities etc.) collected by X-ray surveys at energies below ∼ 8 keV with the CXB spectrum, *under certain assumptions about the spectral energy distribution of AGN in the hard X-ray and soft gamma-ray bands* (from 10 to several hundred keV). This allows one to test the overall paradigm of the CXB being a superposition of AGN and possibly get some hints about still missing (e.g. strongly obscured) populations of AGN or other types of extragalactic objects.

Over the recent years a lot of new observational results have been appearing to constrain this picture. In particular, it has been established how the AGN luminosity function defined at rest-frame energies below 8 keV evolves with redshift, at least out to $z \sim 2$, and there are now constraints on the fraction of obscured AGN as a function of luminosity and redshift (e.g. Ueda et al. 2003; Barger et al. 2005; Tozzi et al. 2006). Most of these data have been obtained in deep, pencil-beam extragalactic surveys conducted by the Chandra and XMM-Newton observatories.

Valuable complementary statistics has recently been provided by shallow hard X-ray surveys of the whole sky performed by RXTE (Revnivtsev et al. 2004; Sazonov & Revnivtsev 2004), Swift (Markwardt et al. 2005), INTEGRAL (Bassani et al. 2006; Beckmann et al. 2006; Krivonos et al. 2007; Sazonov et al. 2007) and HEAO-1 (Shinozaki 2006). Most importantly, these surveys for the first time made it possible to reliably measure the distribution of AGN absorption column densities well into the Compton thick regime ($N_{\rm H} \lesssim 10^{25}$ cm^{-2}), albeit only at low redshifts ($z \lesssim 0.1$). In particular, it was found

Send offprint requests to: sazonov@mpa-garching.mpg.de

that the ratio of obscured ($N_{\rm H} > 10^{22}$ cm^{-2}) to unobscured ($N_{\rm H} < 10^{22}$ cm^{-2}) AGN drops from about 2:1 at hard X-ray (17–60 keV) luminosities below $\sim 10^{43.5}$ erg s^{-1} to about 1:3 at higher luminosities (Sazonov et al. 2007; see also Sazonov & Revnivtsev 2004; Markwardt et al. 2005; Shinozaki 2006).

As was mentioned above, CXB studies so far have usually adopted some fiducial intrinsic AGN spectrum going up to several hundred keV, which was assumed to be similar to the few directly measured spectra of bright nearby Seyfert galaxies (e.g. Jourdain et al. 1992; Zdziarski et al. 1995). However, it has never been demonstrated that *the cumulative hard X-ray spectrum of all AGN residing in a given volume of Universe is compatible with the CXB spectrum*. It is only now that such crucial comparison can be made for the first time, albeit only for the low-redshift AGN population, using the all-sky hard X-ray surveys mentioned above. The IBIS/ISGRI instrument (Ubertini et al. 2003) aboard INTEGRAL (Winkler et al. 2003) is particularly suitable for this purpose since its sensitivity goes effectively up to 300 keV, i.e. well into the energy range where the cumulative AGN spectrum is expected to have a cutoff if our understanding of the CXB is correct.

The purpose of the present work is to estimate the cumulative hard X-ray spectrum of local ($z \lesssim 0.1$) AGN. For this purpose we perform a stacking analysis of the spectra of AGN detected in two recent all-sky surveys, performed by the IBIS/ISGRI instrument aboard INTEGRAL and by the PCA instrument aboard RXTE, taking into account the space densities of AGN with different luminosities (§2). By comparing the derived cumulative AGN spectrum, which spans two decades in energy (3–300 keV), with the CXB spectral energy distribution we obtain constraints on the evolution of AGN in cosmic time (§3). A cosmology with $\Omega_{\rm m} = 0.3, \Omega_\Lambda = 0.7$, and $H_0 = 75$ km s^{-1} Mpc^{-1} is adopted throughout the paper. All quoted uncertainties are 1σ unless noted otherwise.

2. Analysis

We recently used the (mostly) serendipitous all-sky survey conducted by the IBIS/ISGRI instrument (Krivonos et al. 2007) to obtain a sample of nearby AGN detected in the 17–60 keV energy band (Sazonov et al. 2007). This sample is well suited for estimating the cumulative hard X-ray spectrum of local AGN. In what follows we first describe our stacking spectral analysis performed on this AGN set (§2.1). We then report on our similar analysis carried out at lower energies (3–20 keV) using the RXTE Slew Survey (§2.2). Finally we put both sets of results together to obtain a composite AGN spectrum covering the energy range from 3 to 300 keV (§2.3, §2.4).

2.1. INTEGRAL sample

The all-sky survey reported by Krivonos et al. (2007) is based on INTEGRAL/IBIS/ISGRI observations performed during 2002–2006, including a special series of observations of "empty" extragalactic fields. It greatly improves on previous hard X-ray surveys in terms of angular resolution ($\sim 12'$) and sensitivity. For 80% of the sky a flux detection limit of 5 mCrab $\approx 7 \times 10^{-11}$ erg s^{-1} cm^{-2} (17–60 keV) or better is achieved. A total of 403 sources were found, with at most 1–2 of them being spurious.

Nearly two thirds of the sources in the Krivonos et al. (2007) catalog reside in the Galaxy, while the rest are confirmed or suspected AGN. We previously used the INTEGRAL catalog to construct a hard X-ray (17–60 keV) luminosity function of nearby AGN and to study their distribution in absorption column density (Sazonov et al. 2007). As in that work, we now use the subsample of AGN located outside the Galactic plane region ($|b| > 5^\circ$) to avoid problems with identification incompleteness at low Galactic latitudes; our AGN sample is highly complete (at least 92%) at $|b| > 5^\circ$.

In fact the sample of AGN used in the present work is slightly different from that presented by Sazonov et al. (2007) but precisely corresponds to the catalog of Krivonos et al. (2007), which included a few additional INTEGRAL observations and follow-up identifications that became available between those two publications. Specifically, our current sample is composed of 76, rather than 74 AGN detected on the IBIS/ISGRI average sky map at $|b| > 5^\circ$. Information on the two additional sources is presented in Table 1, which should be regarded as a continuation of Table 1 in Sazonov et al. (2007). Among these 76 AGN, there are 8 blazars and 68 nearby ($z \lesssim 0.1$) Seyfert galaxies (although a few of them still lack an exact optical classification). Below we focus on these non-blazar AGN, although a short notice is made in §2.4 with respect to the blazar contribution to the cumulative AGN spectrum.

2.1.1. Reconstruction of multiband sky images

To obtain the hard X-ray spectra of the INTEGRAL AGN we essentially repeated our analysis of IBIS/ISGRI data, previously performed in the 17–60 keV energy band (see Krivonos et al. 2007 for details), in 7 narrow channels: 17–26, 26–38, 38–57, 57–86, 86–129, 129–194 and 194–290 keV. This resulted in time-averaged maps of the whole sky in these energy bands, which were then used to measure source spectral fluxes.

There are two important differences with respect to the Krivonos et al. (2007) study. First, for the present work we updated our data set by adding all IBIS/ISGRI data that became available to us since the last publication. This amounted to 5 Ms of cleaned and deadtime-corrected data in addition to 33 Ms available before. Second, rather than using the entire catalog of Krivonos et al. (2007) in constructing sky maps in the different narrow energy bands, only those sources detectable in a given energy band were used to reconstruct clean sky images in that channel from raw IBIS/ISGRI shadowgrams. This essentially eliminates iterative removal of sources from images, unnecessary in the high-energy channels (129–194 and 194–290 keV), where only 27 and 8 sources, respectively, are detected ($> 5\sigma$) on the whole sky, and reduces the error in measured fluxes.

It is important to emphasize that after the addition of the most recent IBIS/ISGRI data we continue to base our analysis on the original AGN catalog (Sazonov et al. 2007 plus the two sources in Table 1) and the corresponding exposure map from Krivonos et al. (2007). Thus, the new data, added in an attempt to somewhat improve the quality of the source spectra, do not affect the statistical properties of our AGN sample.

When carrying out a stacking analysis like ours one should always worry that some systematic uncertainties associated with the reconstruction of individual source fluxes

Table 1. AGN detected on the average IBIS/ISGRI map at $|b| > 5^\circ$ in addition to the Sazonov et al. (2007) sample

Object	Class[a]	Ref.[b]	z	D[c] Mpc	F_{17-60} 10^{-11} erg s^{-1} cm^{-2}	$\log L_{17-60}$ erg s^{-s}	$N_{\rm H}$ 10^{22} cm^{-2}	Ref.[d]
SWIFT J0601.9−8636=ESO 005-G004	S2	1	0.0062	22.4	2.51 ± 0.46	42.18	~ 100	1
IGR J14561−3738=ESO 386-G034	S2	2	0.0246		1.40 ± 0.26	43.23	?	

[a] Optical AGN class: S2 – Seyfert 2 galaxy.
[b] Reference for the optical classification: (1) Morelli et al. (2006), (2) Masetti et al. (2007).
[c] Distance according to the Nearby Galaxies Catalogue (Tully 1988).
[d] Quoted absorption column density $N_{\rm H}$ is adopted from: (1) Ueda et al. (2007).

may be greatly enhanced by adding up the fluxes of many sources. Therefore, in order to verify that our results do not suffer from systematic uncertainties related to image reconstruction we made a number of simulations.

In particular, we have extracted spectra from 3,000 "empty" positions on the sky chosen in accordance with the INTEGRAL exposure map, i.e. the number density of these "zero-flux" sources was made higher in regions of large exposure than in regions of small exposure. When we carried out simulations including in the iterative source removal procedure all sources from the INTEGRAL catalog, irrespective of the significance of their detection in the considered energy channel, the mean of the distribution of the fluxes of the simulated sources proved to be raised above zero by ~ 0.05–0.1σ (where σ is the typical uncertainty of source flux measurement), which is unacceptable for our stacking analysis. This result is actually anticipated for the employed algorithm of image reconstruction (Krivonos et al. 2007). However, when we repeated the simulations in exactly the same manner as we did our real stacking analysis, i.e. including into our iterative source removal procedure only those INTEGRAL sources that are significantly detected in the considered energy channel, we found that the distribution of the fluxes of the simulated sources is consistent with the normal one with zero mean and the dispersion expected from Poisson statistics.

This proves that a stacking analysis of as many as 3,000 sources does not suffer from any systematic uncertainties in our image reconstruction procedure.

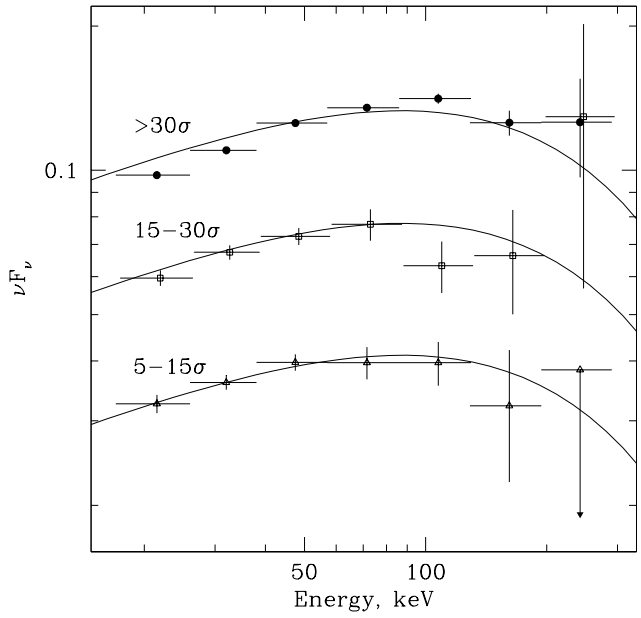

Fig. 1. Average IBIS/ISGRI spectra of non-blazar AGN divided into three groups according to their detection significance in the 17–60 keV energy band. The spectral normalizations are arbitrary. Upper limits are 1σ. The solid lines show crude approximations by the cutoff power law model with $\Gamma = 1.65$ and $E_f = 250$ keV.

2.1.2. Stacked spectra

The individual AGN spectra derived from the reconstructed IBIS/ISGRI multiband sky images are discussed in detail elsewhere (Krivonos et al., in preparation). Here we are interested only in the average properties of these spectra.

We first separately stacked AGN spectra within three groups defined by the source signal-to-noise ratio in the 17–60 keV energy band: > 30 (5 sources), between 15 and 30 (6 sources) and < 15 (57 sources). This is done mainly to avoid that the stacked spectrum is dominated by one or two bright sources. The resulting spectra are shown in Fig. 1. One can see that all three spectra are similar to each other. They exhibit some rollover between ~ 40 and ~ 200 keV and can be approximately described by a power law with a high-energy cutoff: $dN/dE \propto E^{-\Gamma} \exp(-E/E_f)$, with $\Gamma \sim 1.65$ and $E_f \sim 250$ keV (see the solid lines in Fig. 1). This model provides an adequate approximation of the observed spectra, but given the limited energy coverage (17–290 keV), other functional forms (e.g. a broken power law) would fit the INTEGRAL data equally well.

The fact that the averaged spectra of local AGN presented in Fig. 1 have a maximum at energies ~ 80–100 keV, which can be explained by the presence of a high-energy cutoff with $E_f \sim 250$ keV, implies that if the same hard X-ray emission were coming from redshifts $z \sim 1$–2 its spectrum observed at $z = 0$ would have a peak near ~ 30 keV, similar to the cosmic X-ray background. However, these stacked spectra cannot yet be regarded as characteristic of the collective hard X-ray emission of the local AGN population, since neither AGN space densities nor luminosities were taken into account when constructing them.

To really obtain the cumulative spectrum of local AGN, the following weighted stacking should be done:

$$S_i = \sum_j \frac{L_{i,j}}{V_{\rm max,j}} = \sum_j \frac{4\pi D_j^2 F_{i,j}}{V_{\rm max,j}}. \quad (1)$$

Here S_i is the cumulative volume emissivity (measured in units of erg s^{-1} Mpc^{-3}) in energy channel i (from 1 to 7),

$L_{i,j}$ is the luminosity of j'th AGN in channel i, $F_{i,j}$ is the measured flux from j'th AGN in channel i, D_j is the source luminosity distance and $V_{\rm max,j}$ is the volume of space within which an AGN with luminosity L_j in the 17–60 keV band could be detected in the INTEGRAL survey. The source distances (D_j) and signal-to-noise ratios (used to derive the maximum volumes $V_{\rm max,j}$ given the INTEGRAL sky exposure map) are adopted from Sazonov et al. (2007), where the hard X-ray luminosity function of local AGN was derived in a similar way, and also from Table 1. The conversion of detector counts to photon fluxes in the 7 spectral bands was calibrated using IBIS/ISGRI measurements of the Crab and assuming that the Crab spectrum is given by $dN/dE = 10(E/1\ {\rm keV})^{-2.1}$ phot keV^{-1} s^{-1} cm^{-2} (see Krivonos et al., in preparation, for further details).

There are two types of uncertainty associated with the summed spectrum S_i. One results from the errors $\delta F_{i,j}$ in the measured source spectral fluxes (and the associated uncertainties, $\delta L_{i,j} = 4\pi D_j^2 \delta F_{i,j}$, in the spectral luminosities) and is given by:

$$\delta S_{i,1} = \sqrt{\sum_j \left(\frac{\delta L_{i,j}}{V_{\rm max,j}} \right)^2}. \quad (2)$$

Another uncertainty is associated with the finite size of our AGN sample:

$$\delta S_{i,2} = \sqrt{\sum_j \left(\frac{L_{i,j}}{V_{\rm max,j}} \right)^2}, \quad (3)$$

i.e. these uncertainties are associated with the Poisson distribution of detector counts and the number of sources, respectively. Since the first uncertainty is directly linked to the survey's sensitivity in different energy bands, its relative amplitude is much larger for the high-energy channels than for the low-energy ones. In contrast, the second uncertainty is nearly independent of the energy band ($\delta S_{i,2}/S_i \approx$ const) and affects the normalization of the cumulative spectrum rather than its shape.

In Figs. 2 and 3 we show two cumulative AGN spectra obtained using equations (1)–(3). In the first case the stacking was done for the AGN (40 in total) with luminosities between $L_{\rm min} = 10^{41}$ and $L_{\rm max} = 10^{43.5}$ erg s^{-1} (17–60 keV). In the other case, $L_{\rm min} = 10^{43.5}$ erg s^{-1} and $L_{\rm max} = \infty$ (27 AGN). This division approximately corresponds to the low-luminosity and high-luminosity branches of the luminosity function of nearby AGN, which are characterized by different ratios of obscured and unobscured sources (Sazonov et al. 2007) and so may represent somewhat different populations of AGN.

2.2. RXTE/PCA sample

We have thus obtained the cumulative spectral energy distributions of local low-luminosity and high-luminosity AGN in the energy range 17–290 keV. There is an obvious need to continue these spectra to lower energies where intrinsic X-ray absorption in AGN should come into play, producing a low-energy cutoff in the spectra of obscured objects. There are two possible ways to obtain this low-energy part of the cumulative spectrum. One is to search the literature and data archives for X-ray spectra of the INTEGRAL AGN. We decided not to follow this approach for two reasons. First, published or archival X-ray observations of sufficient quality do not exist for all of our objects. Second, because AGN are inherently variable, adding lower-energy spectral fluxes to the IBIS/ISGRI hard X-ray spectra could introduce a bias due to the fact that these particular AGN tended to be detected by IBIS/ISGRI as they were bright relative to their typical flux levels (averaged over many years), while a different X-ray telescope will find the same source equally likely either below or above its average flux level (see Shinozaki 2006 for a detailed discussion of this effect). As a result, the low-energy part of the cumulative spectrum derived by this method might somewhat underestimate the true spectral energy distribution of the local AGN population.

Another feasible approach consists of using an independent survey of nearby AGN performed at the energies of our current interest, i.e. just below 20 keV. Such a survey of the whole sky in the energy band 3–20 keV was recently performed with the PCA instrument aboard the RXTE observatory during its slews between pointed observations –

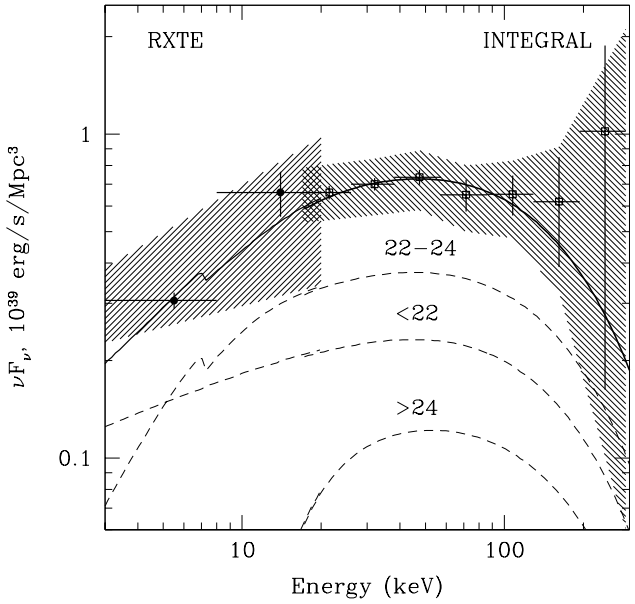

Fig. 2. Cumulative 3–300 keV spectrum of local AGN with luminosities (observed in the 17–60 keV band or absorption corrected in the 3–20 keV band) $10^{41} < L_{\rm hx} < 10^{43.5}$ erg s^{-1}, obtained with INTEGRAL/IBIS/ISGRI and RXTE/PCA. The error bars are 1σ uncertainties of the first type [equation (2)], while the shaded regions show the combined 1σ uncertainties of the first and second type [equation (3)]. The solid line is the best-fit model by a sum of absorbed and unabsorbed power laws with a high-energy exponential cutoff [equation (4), Table 4]. The dashed lines indicate the contributions of unobscured AGN, and obscured AGN with $N_{\rm H} < 10^{24}$ and $> 10^{24}$ cm^{-2}. The RXTE points have been mutliplied by a factor of 1.1 and the INTEGRAL points divided by the same factor to correct for the effect of the local large-scale structure (see §2.2.1).

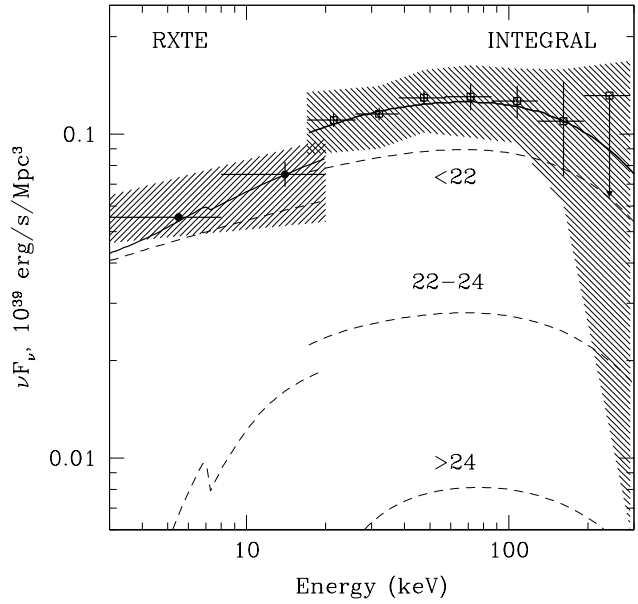

Fig. 3. Same as Fig. 2, but for $L_{\rm hx} > 10^{43.5}$ erg s^{-1}. The upper limit in the highest energy channel is 1σ. No corrections for the local large-scale structure have been done.

the RXTE Slew Survey, or XSS (Revnivtsev et al. 2004). In this survey a flux limit of 1.8×10^{-11} erg s^{-1} cm^{-2} (3–20 keV) or better was achieved for 80% of the sky at $|b| > 10^\circ$. Therefore, the XSS is substantially more sensitive than the IBIS/ISGRI survey with respect to unobscured AGN (e.g. Seyfert 1 galaxies) but is less sensitive with respect to strongly obscured ($N_{\rm H} \gtrsim 10^{23}$ cm^{-2}) ones.

The high Galactic latitude ($|b| > 10^\circ$) part of the XSS was previously used to obtain a catalog of AGN, to construct the 3–20 keV luminosity function of nearby AGN and to study their distribution of absorption column densities (Sazonov & Revnivtsev 2004), quite similarly to the analysis of the INTEGRAL survey we carried out later. Here we use the XSS to obtain low-energy intensities for our cumulative hard X-ray spectra of local AGN.

Since the original XSS publications several changes have taken place that need to be taken into account here. First, originally a substantial fraction ($\sim$ 30%) of XSS sources were unidentified, mainly because of their poor localization (uncertainty up to 1°). Over the passed three years many of these sources have been identified, thanks to dedicated follow-up efforts (Bikmaev et al. 2006; Revnivtsev et al. 2006; Landi et al. 2007) or due to detection and improved localization of some of these sources by INTEGRAL or Swift. As a result, the XSS sample of AGN detected ($> 4\sigma$) at $|b| > 10^\circ$ is now composed of 103, rather than 95 sources, including 84 non-blazar AGN. The new non-blazar AGN are listed in Table 2, which should be considered a continuation of Table 1 in Sazonov & Revnivtsev (2004). At the same time the number of unidentified XSS sources (detected at $> 4\sigma$) has decreased to 16 objects. Therefore, the XSS AGN sample is now at least 82% complete[1], so incompleteness is less of a problem than before.

Secondly, through careful testing of our methods developed for analyzing data recorded in the slew mode of RXTE observations we found that the conversion factors from PCA counts to source photons quoted in Revnivtsev et al. (2004) were underestimated by a factor of $\sim 1/0.7$, because we had not taken into account that the PCA field of view is rapidly moving across sources during RXTE slews and used a slow movement approximation of the PCA response. This implies that, to first approximation, the AGN luminosities quoted in Sazonov & Revnivtsev (2004) should be revised upwards by a factor of 1/0.7 (the same correction factor applies to Table 2 presented here).

There are a few other minor modifications that have been implemented, including the correction of a misprint in Sazonov & Revnivtsev (2004) for the redshift of NGC 7582 from 0.053 to 0.0053 and accordingly revising its luminosity.

We plan to release an updated version of the XSS catalog in the near future, including the modifications described above and possibly a number of additional source identifications.

It is important to note that although the RXTE and INTEGRAL AGN samples are comparable in size, they overlap by just $\sim$ 30%, i.e. these samples are mostly independent of each other. Although this result may seem unexpected, it can readily be explained by a combination of circumstances: 1) the XSS catalog is defined at $|b| > 10^\circ$, whereas the INTEGRAL AGN sample used here is defined at $|b| > 5^\circ$ and the strip of the sky between $|b| = 5^\circ$ and $|b| = 10^\circ$ is well covered by INTEGRAL observations, 2) the distribution of exposure over the sky is significantly different for the two surveys, 3) due to its lower energy band the XSS is biased toward detecting unobscured and weakly obscured AGN and against detecting Compton thick AGN, 4) AGN are inherently variable and the two surveys were conducted at significantly different epochs.

We used the updated XSS AGN sample to obtain the 3–8 and 8–20 keV points for our cumulative hard X-ray spectra of local low-luminosity and high-luminosity AGN (Figs. 2 and 3) following the same $1/V_{\rm max}$ weighted summing method as we used above (§2.1) to obtain the high-energy parts of the spectra based on IBIS/ISGRI data. We note that the XSS sample includes 6 non-blazar AGN located at $z \sim 0.15$–0.3. Nonetheless, since the vast majority of the sample are truly local sources ($z \lesssim 0.1$) and the several more distant AGN contribute just a few per cent to the resulting cumulative spectra, we included these objects in our stacking analysis as if they were local, i.e. ignoring any evolution of AGN between $z = 0.3$ and $z = 0$.

There are three differences with respect to our analysis of the IBIS/ISGRI data, all caused by the strong effect of intrinsic absorption on AGN spectra below 20 keV. First, in determining the $V_{\rm max}$ values for the XSS sources, we took into account their absorption column densities given in Table 1 in Sazonov & Revnivtsev (2004) and in Table 2 presented here. That is $V_{\rm max}$ is now defined as the volume of space in which the XSS would detect an AGN with its observed 3–20 keV luminosity and column density $N_{\rm H}$ (not just the luminosity as in the INTEGRAL case). Second, the $N_{\rm H}$ values were taken into account also to calculate

[1] Here it is also taken into account that ~ 6 additional AGN are possibly confused with other XSS sources.

Table 2. Non-blazar AGN detected at $|b| > 10^\circ$ during the RXTE Slew Survey in addition to the Sazonov & Revnivtsev (2004) sample

XSS object (J2000.0)	Name	Class[a]	Ref.[b]	3–8 keV cnt s^{-1}	8–20 keV cnt s^{-1}	z	log L_{3-20}[c] erg s^{-1}		N_H 10^{22} cm^{-2}	Ref[d]
05054−2348	2MASX J05054575−2351139	S2	1	0.69 ± 0.19	0.92 ± 0.23	0.0350	43.77	43.83	6	1
12303−4232	IRAS F12295−4201	S1.5	2	0.48 ± 0.09	0.29 ± 0.11	0.1000	44.37	44.37	< 1	1
12389−1614	2MASX J12390630−1610472	S2	3	0.93 ± 0.11	0.51 ± 0.13	0.0367	43.75	43.77	2	2
15076−4257	2MASX J15080462−4244452	S1	4	0.73 ± 0.05	0.24 ± 0.06	0.0565	43.96	43.96	< 1	3
18236−5616	IC 4709	S2	5	0.32 ± 0.09	0.51 ± 0.12	0.0169	42.86	42.98	12	1
19459+4508	2MASX J19471938+4449425	S2	1	0.38 ± 0.10	0.38 ± 0.12	0.0532	43.84	43.95	11	2
21354−2720	IRAS F21318−2739	S1.5	1	0.41 ± 0.11	0.32 ± 0.13	0.0670	43.99	43.99	< 1	4

[a] Optical AGN class: S1.5 – Seyfert 1.5 galaxy, S2 – Seyfert 2 galaxy.
[b] Reference for the optical classification: (1) Bikmaev et al. (2006), (2) Landi et al. (2007), (3) Masetti et al. (2006a), (4) a Seyfert 1 nucleus is suggested by the 6dF spectrum, (5) Masetti et al. (2006b).
[c] Left and right columns give the observed and absorption corrected luminosities in the 3–20 keV band, respectively.
[d] Quoted absorption column density value is adopted from or based on: (1) Revnivtsev et al. (2006),(2) Sazonov et al. (2005), (3) ROSAT data, (4) Swift data.

the observed and intrinsic (corrected for the absorption) luminosities of the XSS AGN in the subbands 3–8 and 8–20 keV from the detector counts measured in these channels (as given in Table 1 in Sazonov & Revnivtsev (2004) and in Table 2 presented here). In doing this conversion the source spectrum was assumed to have an intrinsic slope of 1.8, although the result only weakly depends on this assumption (Revnivtsev et al. 2004). And finally, we used the same two luminosity ranges: 1) $L_{\rm min} = 10^{41}$, $L_{\rm max} = 10^{43.5}$ erg s^{-1} (38 AGN) and 2) $L_{\rm min} = 10^{43.5}$, $L_{\rm max} = \infty$ (46 AGN), as for our stacking analysis of INTEGRAL spectra, but for RXTE these ranges are defined for absorption-corrected luminosities in the 3–20 keV energy band. This ensures that the stacking of both INTEGRAL and RXTE spectra is done for almost identical populations of AGN, since the unabsorbed luminosities of AGN in the 3–20 keV and 17–60 keV bands are very similar (see e.g. Fig. 7 in Sazonov et al. 2007).

2.2.1. Influence of the local large-scale structure

Both the INTEGRAL and RXTE all-sky surveys are characterized by substantially nonuniform coverage of the sky. Furthermore, the sky exposure maps of these surveys are quite different. Because both surveys effectively picked out AGN within $\sim$ 100–200 Mpc from us and the distribution of matter in the local Universe is inhomogeneous, effects of the local large-scale structure may come into play when comparing AGN space densities or any quantities depending thereof (luminosity functions, cumulative spectral energy distribution etc.) estimated using one survey and the other. It is straightforward to estimate these effects if we assume that AGN are distributed in the local Universe approximately as normal galaxies. Krivonos et al. (2007) have actually demonstrated that the AGN detected by INTEGRAL do follow quite well the spatial distribution of galaxies.

To assess the effect of the local large-scale structure on the cumulative spectra of low-luminosity and high-luminosity AGN (Figs. 2 and 3), we made use of the IRAS PSCz catalog (Saunders et al. 2000), which is the most complete published all-sky galaxy redshift catalog. Our analysis essentially consisted of counting PSCz galaxies within the volume of space in which the INTEGRAL or RXTE survey can detect AGN with a given hard X-ray (3–20 or 17–60 keV) luminosity, and calculating the average matter density in that part of the Universe. In reality, the situation is somewhat more complicated, first because the INTEGRAL and RXTE surveys are nonuniform, hence the distance out to which a source with a given luminosity is detectable depends on the direction in the sky, and also because the PSCz catalog itself becomes incomplete at a certain distance that depends on galaxy infrared luminosity. Nonetheless, it is easy to take these effects into account to first approximation.

Fig. 4 summarizes the results of our analysis carried out along the above lines. In the upper panel shown are the space densities of galaxies with infrared (60 μm) luminosities exceeding certain limits $L_{\rm IR,\ cut}$ and located within the volume of space $V(L_{\rm hx})$ probed by either INTEGRAL or RXTE as a function of AGN hard X-ray luminosity $L_{\rm hx}$ (17–60 keV or 3–20 keV). In the lower panel, the ratio of the INTEGRAL and RXTE specific densities is plotted. Note that the sky below $|b| = 10^\circ$ was excluded from the analysis, even though our INTEGRAL AGN sample goes down to $|b| = 5^\circ$, to avoid problems with incompleteness of the PSCz catalog at low Galactic latitudes (Saunders et al. 2000). For simplicity, in calculating $V(L_{\rm hx})$ we assumed a power-law spectrum with a photon index of 1.8. Nine values of $L_{\rm IR,\ cut}$ are chosen: 5×10^8, 10^9, 2×10^9, 5×10^9, 10^{10}, 2×10^{10}, 5×10^{10}, 10^{11} and $2 \times 10^{11} L_\odot$. Since the PSCz catalog is highly complete at 60 μm fluxes higher than 0.6 Jy (Saunders et al. 2000), except near the Galactic plane, these limiting IR luminosities approximately correspond (we ignore here any k-corrections since we are dealing with low redshifts) to distances $D_{\rm max} = 23$, 32, 45, 72, 102, 144, 228, 322 and 455 Mpc, within which the chosen subsamples of PSCz galaxies are expected to be complete. For each of these sets of galaxies we show in Fig. 4 their space densities estimated within the INTEGRAL and RXTE survey volumes for such $L_{\rm hx}$ that $D_{\rm max}(L_{\rm IR,\ cut}) \geq D_{90}(L_{\rm hx})$, where D_{90} is the distance within which 90% of the space volume probed by INTEGRAL or RXTE at $L_{\rm hx}$ is contained. This combination of dwarf, normal and giant IRAS galaxies allows us to compare the average matter densities characteristic of the INTEGRAL and RXTE surveys in the broad range of AGN luminosities of our interest.

Fig. 4 indicates that the local volume of Universe probed by INTEGRAL at $L_{\rm hx} \lesssim 10^{43.5}$ erg s^{-1} is a factor of ~ 1.2 denser than the corresponding volume probed by RXTE. A comparison of the sky exposure maps of INTEGRAL (Krivonos et al. 2007) and RXTE (Revnivtsev et al. 2004)

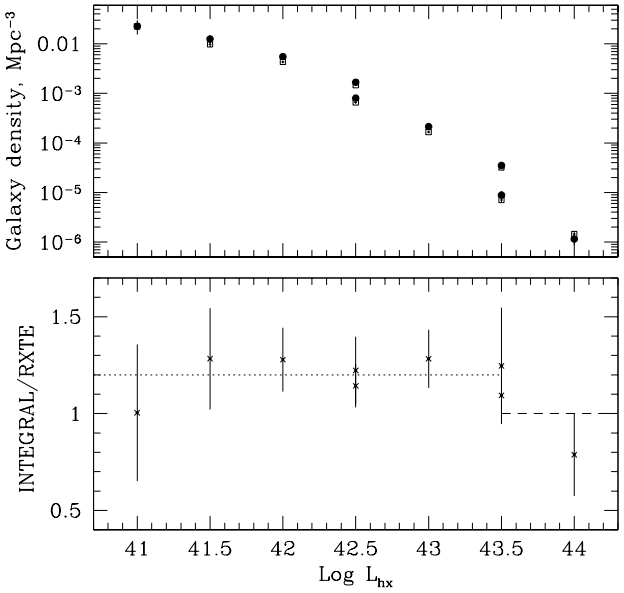

Fig. 4. *Upper panel:* Average galaxy number density within the space volume probed at $|b| > 10^\circ$ by INTEGRAL (filled points) and RXTE (open points) as a function of AGN hard X-ray luminosity. A number of IRAS PSCz galaxy 60-μm luminosity cuts are used (from top to bottom): 5×10^8, 10^9, 2×10^9, 5×10^9, 10^{10}, 2×10^{10}, 5×10^{10}, 10^{11} and $2\times10^{11} L_\odot$. *Lower panel:* Ratio of the densities in the INTEGRAL and RXTE volumes as a function $L_{\rm hx}$. Also shown are the typical ratios, 1.2 and 1.0, at $L_{\rm hx} < 10^{43.5}$ (dotted line) and $L_{\rm hx} > 10^{43.5}$ erg s^{-1} (dashed line), respectively, which are adopted as correction factors for the cumulative spectra of low- and high-luminosity AGN, respectively.

provides a likely explanation for this: while INTEGRAL has spent a lot of time observing such major local large-scale structures as the Centaurus cluster–Shapley supercluster and the Perseus–Pisces supercluster, the RXTE Slew Survey has relatively low exposure in these regions. On the other hand, we do not find (see Fig. 4) any significant difference in the average matter densities of the INTEGRAL and RXTE survey volumes at higher AGN luminosities ($L_{\rm hx} \gtrsim 10^{43.5}$). This is also an expected result, since high-luminosity AGN are typically observed by INTEGRAL and RXTE at distances larger than 100 Mpc and on such spatial scales the Universe is already close to being homogeneous.

To take into account to first approximation the apparent effect of the local large-scale structure, we multiplied the RXTE points of the cumulative spectrum of low-luminosity AGN (Fig. 2) by a factor of 1.1 and divided the INTEGRAL points by the same factor. No such corrections have been done for the cumulative spectrum of high-luminosity AGN (Fig. 3).

Table 3. Relative fractions of local AGN with different absorption column densities at low and high luminosities, adopted from Sazonov et al. (2007)

$\log N_{\rm H} < 22.0$	k ($\log L_{\rm hx} \lesssim 43.5$)	k ($\log L_{\rm hx} \gtrsim 43.5$)
< 22.0	0.32	0.76
22.0–22.5	0.19	0.05
22.5–23.0	0.05	0.00
23.0–23.5	0.12	0.05
23.5–24.0	0.15	0.14
24.0–24.5	0.10	0.00
> 24.5	0.07	0.00

2.3. Spectral modeling

We next modeled, using XSPEC (Arnaud 1996), the broad-band (3–300 keV) cumulative spectral energy distributions of local low- and high-luminosity AGN obtained in the previous sections by a sum of absorbed and unabsorbed power-law spectra with a high-energy exponential cutoff:

$$E^2 dN/dE = A \sum_i k_i f(N_{\rm H,i}) E^{-\Gamma+2} \exp(-E/E_f). \qquad (4)$$

This model is by definition a sum of identical spectra absorbed by different column densities $N_{\rm H,i}$ of neutral gas: 0, $10^{22.25}$, $10^{22.75}$, $10^{23.25}$, $10^{23.75}$, $10^{24.25}$ and $10^{24.75}$ cm^{-2}. We fix the weights k_i ($\sum k_i = 1$) of these columns at the relative fractions of AGN with different $N_{\rm H}$ as measured by INTEGRAL (Sazonov et al. 2007), ignoring the associated uncertainties. The corresponding fractions at low ($L_{\rm hx} \lesssim 10^{43.5}$ erg s^{-1}) and high ($L_{\rm hx} \gtrsim 10^{43.5}$ erg s^{-1}) luminosities are given in Table 3. We use them accordingly for modeling the cumulative spectra of low- and high-luminosity AGN (Fig. 2 and Fig. 3).

The photoabsorption modifiers $f(N_{\rm H,i})$ are determined using the XSPEC model phabs assuming solar element abundances. Note that for substantially Compton thick sources ($N_{\rm H} \gtrsim 10^{24.5}$ cm^{-2}) this simple photoabsorption model becomes inadequate, but since the relative fraction of such sources according to the INTEGRAL survey is small ($\lesssim 10\%$) we apply this model to all AGN.

The free parameters of our model are the power-law slope Γ, the position of the high-energy cutoff E_f and the normalization A, which is allowed to take different values for the RXTE and INTEGRAL parts of the spectrum to avoid a situation where some systematic effects, e.g. associated with the cross-calibration of the IBIS/ISGRI and PCA detectors or with the local large-scale structure (see §2.2.1), would affect the modeling of the spectral shape. At the same time this allows us not to take into account the uncertainties associated with the finite sizes of the INTEGRAL and RXTE AGN samples [equation (3)] when fitting the spectrum, since these uncertainties are strongly correlated between the different energy channels for a given survey and do not affect the spectral shape. We do however consider these errors when we discuss the final spectral normalization below.

The above model provides an excellent fit to both the cumulative spectrum of low-luminosity AGN and to that of high-luminosity AGN. The best-fit parameter values are given in Table 4 and the associated confidence regions for the two main parameters Γ and E_f are shown in Figs. 5 and 6. The best-fit models are shown in Figs. 2 and 3, as well as

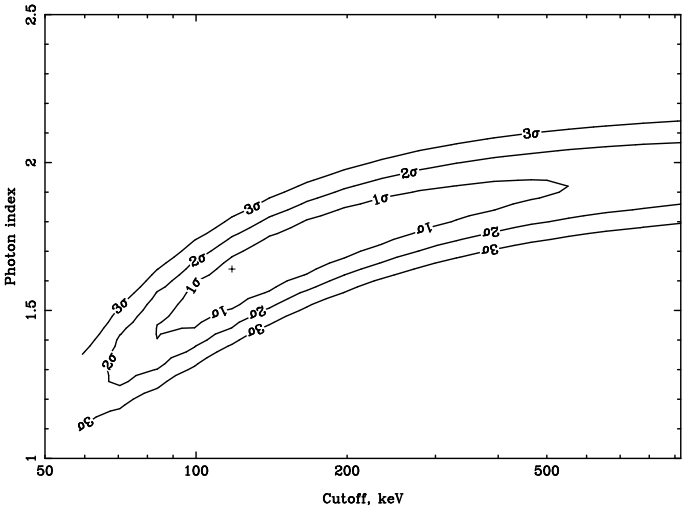

Fig. 5. Confidence regions for the power-law slope Γ and position of the high-energy cutoff E_f in the model [equation (4)] for the cumulative spectrum of low-luminosity ($10^{41} < L_{\rm hx} < 10^{43.5}$ erg s^{-1}) AGN. The position of the best-fit parameter values is indicated by the cross.

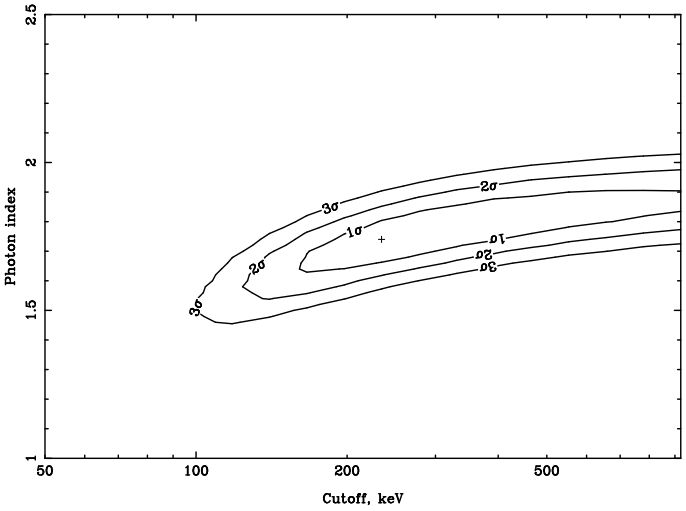

Fig. 6. Same as Fig. 5, but for the cumulative spectrum of high-luminosity AGN ($L_{\rm hx} > 10^{43.5}$ erg s^{-1}).

the contributions of unobscured ($\log N_{\rm H} < 22$), obscured ($22 < \log N_{\rm H} < 24$) and heavily obscured ($\log N_{\rm H} > 24$) AGN to the total spectra.

In summary, the best-fit power-law photon index is found to be $\sim$ 1.7, as expected of AGN (see e.g. Reynolds et al. 1997; Turner et al. 1997). In both studied cases, the model prefers to have a high-energy cutoff with $E_f \sim$ 100–300 keV, while its detection is only marginal ($< 2\sigma$) in both cases. Previously, similar values of the cutoff energy have been inferred from individual spectra of several brightest Seyfert galaxies (in particular, NGC 4151), selected without regard to their luminosities or space densities, as well as upon averaging over such spectra (e.g. Jourdain et al. 1992; Zdziarski et al. 1995; Perola et al. 2002; Molina et al. 2006).

We point out that the apparent small ($\sim 20\%$) difference in the normalizations of the low-energy (RXTE) and high-energy (INTEGRAL) parts of the cumulative spectrum of high-luminosity AGN is fully consistent with the uncertainties associated with the finite size of the INTEGRAL and RXTE samples (see the second set of uncertainties on the corresponding A values in Table 4). The total 1σ spectral uncertainties are shown as shaded regions in Figs. 2 and 3 and one can see that the INTEGRAL and RXTE data are in good agreement with each other.

We note that apart from the relatively simple model given by equation (4) we also tried to fit the measured spectra by more complicated models. In particular we tried adding a Compton reflection component. Since this did not lead to a significant improvement of the quality of the fit nor it provided interesting constraints on the amplitude of the reflection component (due to its strong correlation with the power-law slope and the position of the high-energy cutoff), we base all of the remaining discussion on our model of a sum of absorbed and unabsorbed power-law spectra with a high-energy cutoff.

2.4. Cumulative spectrum of the local AGN population

We have seen that the shapes of the summed spectra of low- and high-luminisity AGN are similar to each other except that the spectrum is harder below 20 keV in the former case due to the larger fraction of obscured sources at low luminosities ($L_{\rm hx} \lesssim 10^{43.5}$ erg s^{-1}). We can now finally determine the spectral energy distribution of the hard X-ray volume emissivity of all local AGN with luminosities over 10^{41} erg s^{-1}.

To this end, we first slightly rescale the best-fit spectral models presented above. Specifically, we define the amplitudes of the low- and high-luminosity spectral components to be the averages between the corresponding INTEGRAL and RXTE values given in Table 4, so that

$$A_{\rm low} = 2.7 \times 10^{38} \text{ erg s}^{-1} \text{ Mpc}^{-3} \quad (5)$$

and

$$A_{\rm high} = 0.49 \times 10^{38} \text{ erg s}^{-1} \text{ Mpc}^{-3}. \quad (6)$$

In Fig. 7 we show by the solid line the sum of our low- and high-luminosity best-fit models with the normalizations given by equations (5) and (6). This is our best estimate of the cumulative spectrum of local AGN. The vertically hatched region represents the multifold of spectral models that are consistent with the INTEGRAL and RXTE data to within 1σ. The horizontally hatched region represents an additional 20% uncertainty on the overall spectral normalization, which is our estimate of a combination of several uncertainties, which were already discussed in different sections of the paper, namely associated with 1) the finite size of the INTEGRAL and RXTE samples of AGN, 2) the local large-scale structure (although we have taken it into account to first approximation) and 3) possible incompleteness of both AGN samples. The dashed and dotted lines show the contributions of the low-luminosity ($10^{41} < L_{\rm hx} < 10^{43.5}$ erg s^{-1}) and high-luminosity ($L_{\rm hx} > 10^{43.5}$ erg s^{-1}) AGN, respectively. We note that the latter contribute just $\sim 15\%$ to the total local AGN spectrum.

We finally note that blazars are not expected to contribute more than several per cent to the local hard X-ray emissivity at different energies below ~ 200 keV (see Fig. 7). We made this estimate using the same $1/V_{\rm max}$ method that

Table 4. Results of the modeling of the cumulative spectra of low- and high-luminosity AGN

$L_{\rm hx}$ erg s^{-1}	Γ	E_f keV	A (INTEGRAL) 10^{38} erg s^{-1}Mpc^{-3}	A (RXTE)	χ^2/d.o.f.
10^{41}–$10^{43.5}$	1.64 ± 0.17	124^{+134}_{-38}	$2.7 \pm 1.3 \pm 0.5$	$2.7 \pm 0.6 \pm 0.6$	3.7/5
$> 10^{43.5}$	1.74 ± 0.08	258^{+277}_{-79}	$0.55 \pm 0.12 \pm 0.12$	$0.44 \pm 0.06 \pm 0.07$	3.1/5

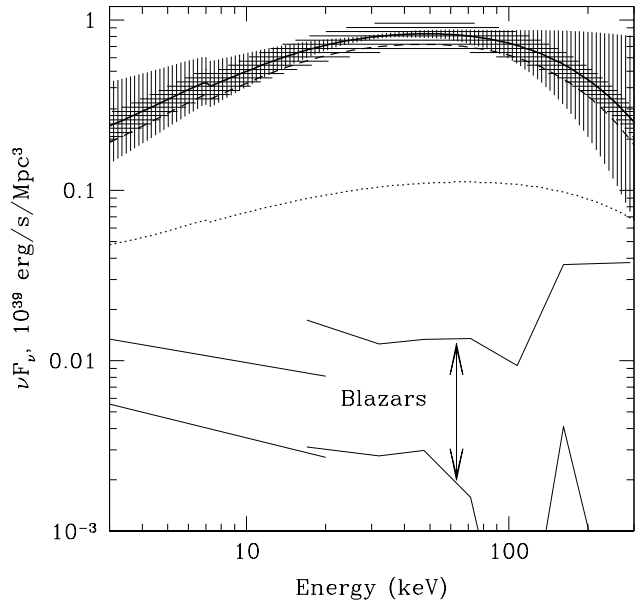

Fig. 7. Cumulative spectrum of local non-blazar AGN with luminosities over 10^{41} erg s^{-1}. The solid line is our best estimate of this spectrum based on INTEGRAL and RXTE data. The vertically hatched region represents the multifold of spectral models that are consistent with the data to within 1σ. The horizontally hatched region represents an additional 20% uncertainty on the overall spectral normalization due to a combination of a number of systematic effects discussed in the text. The dashed and dotted line show the contributions of low-luminosity ($10^{41} < L_{\rm hx} < 10^{43.5}$ erg s^{-1}) and high-luminosity ($L_{\rm hx} > 10^{43.5}$ erg s^{-1}) AGN, respectively. The two solid curves at the bottom of the plot demonstrate the contribution of blazars to the total local emissivity at different energies, estimated based on INTEGRAL and RXTE data, with the distance between the curves corresponding to the 1σ uncertainty.

we used to derive the cumulative spectrum of non-blazar AGN. Although in making this estimate we did not exclude high-redshift flat-spectrum radio quasars present in the INTEGRAL and RXTE catalogs, it is essentially based on the 2 and 9 nearby ($z < 0.1$) BL Lacs detected by INTEGRAL and RXTE, respectively. We also note that the contribution of blazars may well be much more significant in gamma-rays ($E \gtrsim 200$ keV), since emission from blazars can extend to very high energies, in contrast to normal Seyfert galaxies and quasars.

3. Comparison with the cosmic X-ray background

In the previous section we derived the cumulative hard X-ray spectrum of local AGN. Specifically, we determined both its normalization, i.e. the local volume hard X-ray emissivity due to AGN, and shape, which was shown to be well described by a sum of absorbed and unabsorbed power-law spectra with a high-energy cutoff. It is interesting to put these results into the broader perspective of the cosmic history of growth of massive black holes and the origin of the cosmic X-ray background.

To this end, suppose that the shape of the cumulative spectral energy distribution of AGN does not evolve with redshift, which implies a constant relative contribution of obscured sources, while the spectral normalization, i.e. the AGN luminosity density, does experience evolution. The collective emission of AGN from all redshifts observed at $z = 0$ will then have the spectrum (for a flat cosmoslogy)

$$I(E) = \frac{c}{4\pi H_0} \int_0^\infty \frac{\epsilon(z) S((1+z)E)}{(1+z)\left[\Omega_{\rm m}(1+z)^3 + \Omega_\Lambda\right]^{1/2}} dz, \qquad (7)$$

where $S(E)$ is the local cumulative AGN spectrum (Fig. 7) and $\epsilon(z)$ is a function describing the evolution of the AGN luminosity density.

Following Sazonov et al. (2007), we assume that the AGN hard X-ray luminosity density evolves similarly to the AGN 2–8 keV luminosity density as reported by Barger et al. (2005), specifically that $\epsilon(z)$ is bound between two limiting functions:

$$\epsilon_1(z) \propto \begin{cases} (1+z)^{3.2}, & z \le 1 \\ \epsilon_1(1)/z, & z > 1 \end{cases} \qquad (8)$$

and

$$\epsilon_2(z) \propto \begin{cases} (1+z)^{3.2}, & z \le 1 \\ \epsilon_2(1), & z > 1 \end{cases} \qquad (9)$$

This formulation reflects the significant uncertainty in our knowledge of the AGN evolution at $z \gtrsim 1$, whereas the approximately power-law rapid evolution between $z = 0$ and $z \sim 1$ is well established.

We now use equation (7) to convolve our locally determined composite AGN spectrum (Fig. 7) with the two limiting evolution functions, ϵ_1 and ϵ_2. The resulting spectral energy distributions, representing the collective emission of AGN from all redshifts, are shown in Fig. 8 and Fig. 9, respectively. The vertically hatched 1σ-uncertainty regions in these figures have been propagated from the corresponding region in Fig. 7. Similarly, the horizontally hatched regions indicate our estimated 20% uncertainty in the volume emissivity of local AGN propagated to the redshift-integrated spectrum. The calculated spectra in Fig. 8 and 9 are compared with the CXB spectrum measured by INTEGRAL (Churazov et al. 2007).

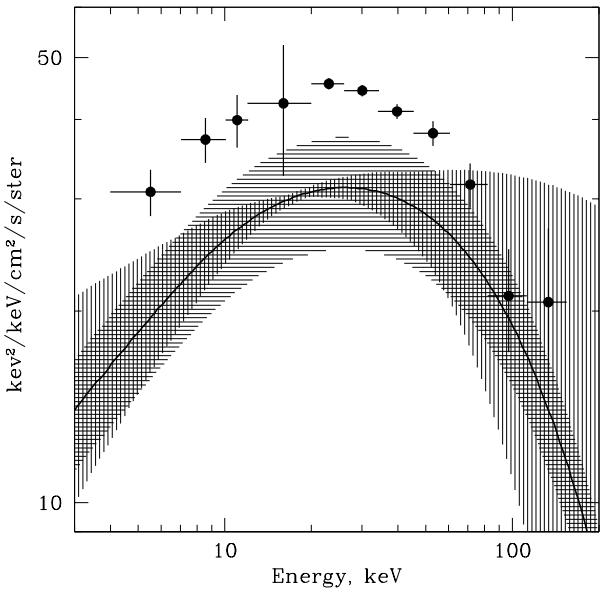

Fig. 8. Result of convolution of the local cumulative AGN spectrum (Fig. 7) with the redshift evolution of the AGN luminosity density described by equation (8). The solid line is our best estimate of this redshift-integrated AGN spectrum. The vertically hatched region represents the associated 1σ statistical uncertainty, whereas the horizontally hatched region represents the additional 20% systematic uncertainty in the overall normalization. The points with error bars show the CXB spectrum measured with the JET-X, IBIS/ISGRI, and SPI instruments on INTEGRAL (Churazov et al. 2007).

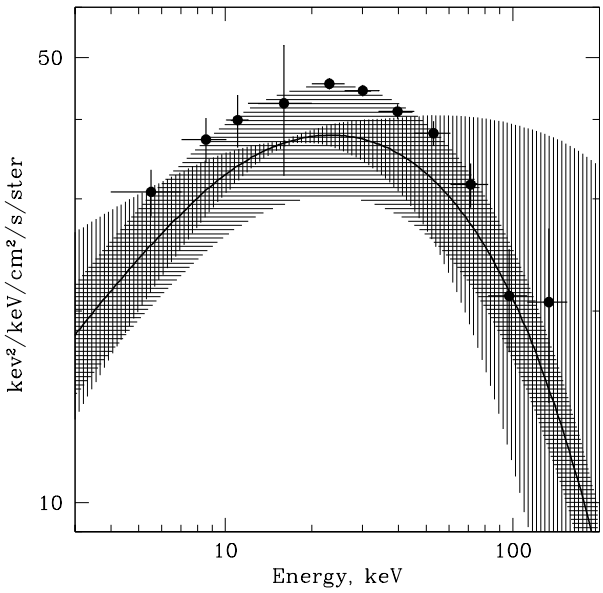

Fig. 9. Same as Fig. 9, but for the scenario of evolution given by equation (9).

It can be seen that within the fairly large uncertainties the shape of the predicted cumulative AGN spectrum is in good agreement with that of the CXB for both limiting scenarios of AGN evolution at $z > 1$ and therefore for the real evolution, which is constrained between $\epsilon_1(z)$ and $\epsilon_2(z)$. As concerns the normalization, depending on the character of evolution at $z > 1$ our model is between being consistent with the observed CXB intensity (in the case of $\epsilon_2(z)$) and underestimating it by some 30% (in the case of $\epsilon_1(z)$).

In fact, if the simple scenario of evolution considered here is correct, we may expect the predicted spectrum to somewhat understimate the CXB intensity. Indeed, the calculation above rested on our estimate of the local AGN emissivity, which was done for non-blazar AGN with luminosities over 10^{41} erg s^{-1}. An additional significant contribution is expected to come from AGN with still lower luminosities ($L_{\rm hx} < 10^{41}$ erg s^{-1}) (Elvis et al. 1984) as well as from blazars (see §2.4 above).

We finally note that if AGN had not undergone any luminosity density evolution, only $\sim 20\%$ of the CXB could be explained. This is illustrated by Fig. 10, where we repeated the above calculations assuming $\epsilon(z) = 1$.

4. Discussion and conclusions

In this paper we used the INTEGRAL and RXTE all-sky hard X-ray surveys to calculate the spectral energy distribution of the collective emission of local AGN in the broad

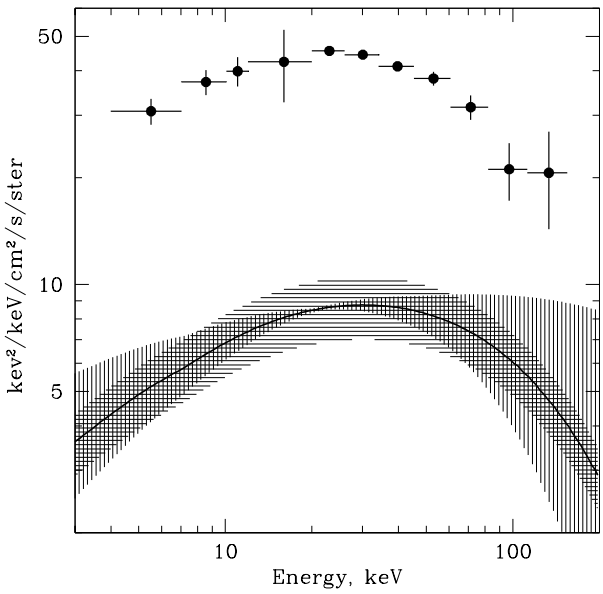

Fig. 10. Same as Fig. 9, but in the case of no AGN evolution.

energy range 3–300 keV, properly taking into account the relative contributions of AGN with different luminosities and absorption column densities.

We first performed stacking spectral analyses separately for AGN with low ($10^{41} < L_{\rm hx} < 10^{43.5}$ erg s^{-1}) and high ($L_{\rm hx} > 10^{43.5}$ erg s^{-1}) luminosities and found that their corresponding cumulative spectra are consistent with having the same shape at energies above 20 keV – in particular both spectra indicate, albeit with low significance, the presence of a high-energy cutoff at energies above ∼100–200 keV, whereas the cumulative spectrum of low-luminosity AGN is harder at energies below 20 keV due to the larger fraction of obscured AGN compared to higher luminosities. We then summed our model approximations for these cumulative spectra of low- and high-luminosity AGN to obtain the spectral energy distribution of all local AGN (excluding blazars) with $L_{\rm hx} > 10^{41}$ erg s^{-1} and estimated the associated statistical and systematic uncertainties.

In an attempt to apply the local cumulative AGN spectrum in the broad context of black hole growth in the Universe, we demonstrated that the cosmic X-ray background spectrum is consistent with the local cumulative AGN spectrum if AGN evolve with cosmic time in such a way that their collective high-energy emission has a constant spectral shape and also the relative fraction of obscured sources remains constant, while the total AGN luminosity density undergoes strong evolution between $z \sim 1$ and $z = 0$. Furthemore, we mentioned that although this simple model underpredicts the observed CXB intensity by $\sim$ 0–30% (depending on the fairly uncertain evolution of AGN at $z \gtrsim 1$), the missing flux can possibly be attributed to the contribution to the hard X-ray emissivity from low-luminosity AGN ($L_{\rm hx} \lesssim 10^{41}$ erg s^{-1} at $z = 0$ and $L_{\rm hx} \lesssim 10^{42}$ erg s^{-1} at $z = 1$–2), which are known to be abundant and energetically important in the local Universe but are not taken into account in the current model. Furthermore, we can extend this argument to conclude that low-luminosity AGN, which are undetectable even in the deepest extragalactic surveys with Chandra and XMM-Newton, cannot provide a dominant contribution to the X-ray emissivity of the Universe at redshifts $z \sim 1$–2, otherwise they would produce too much X-ray background.

How does this assumed scenario of AGN evolution compare with observational data obtained by X-ray telescopes at energies below $\sim$ 8 keV? First of all, a number of studies have shown that AGN have undergone approximately pure luminosity evolution between $z \sim 1$ and $z = 0$ (Ueda et al. 2003; Barger et al. 2005), which means that the AGN luminosity function has shifted to the left (lower luminosities) by nearly an order of magnitude. More fundamentally, it has been demonstrated that black hole growth and galaxy formation have been moving steadily and in parallel to lower and lower mass scales since a redshift of $\sim$ 2 (e.g. Heckman et al. 2004).

This picture of "cosmic downsizing" or " antihierarchical evolution" is consistent with the scenario considered in this paper and in fact in our calculations we adopted the AGN luminosity density evolution between $z = 0$ and $z \sim 1$ from X-ray surveys. As concerns the relative contribution of obscured AGN to the cumulative hard X-ray emissivity at a given redshift, which should be constant in our model, observations seem to indicate that there is indeed no significant evolution in this fraction between $z = 0$ and $z \sim 1$ (Ueda et al. 2003). Therefore, all the available observational data obtained for AGN at $z \lesssim 1$ appear to fit well in the simple scenario of evolution considered in this paper.

However, X-ray observations also suggest that the character of AGN evolution changes at higher redshifts ($z \gtrsim 1$). Namely, the observed AGN evolution is much better described by a luminosity dependent density evolution model, rather than by a pure luminosity evolution one (Ueda et al. 2003; La Franca et al. 2005; Gilli et al. 2007). Also the relative contribution of obscured sources to the total AGN luminosity density may have undergone substantial evolution at $z \gtrsim 1$, although this remains a very controversial issue (La Franca et al. 2005; Akylas et al. 2006; Tozzi et al. 2006; Treister & Urry 2006). Although the different character of AGN evolution at high redshifts with respect to $z < 1$ suggests that our simple model needs to be modified, such a revision would remain almost unnoticed in view of the fairly large uncertainties in our local cumulative AGN spectrum, since, as we have seen in §3, the current uncertainty in the AGN evolution at $z > 1$ leads to less than $\sim$ 30% uncertainty in the predicted CXB spectrum, which is of the same order as the uncertainties in the cumulative spectrum of local AGN obtained from INTEGRAL and RXTE data.

We also note that it is possible that in reality the hard X-ray spectra of distant quasars are somewhat different from those of the nearby Seyfert galaxies that make up our local cumulative spectrum, since, although AGN spectra are not expected to directly depend on cosmological redshift, they can depend on physical parameters of the accretion disk around the central massive black hole, determined by the black hole mass, accretion rate (Shakura & Sunyaev 1976) and spin. Observations with future hard X-ray telescopes will permit direct tests of whether the high-energy spectra of quasars are similar to those of local AGN or not.

The main result of this work is that for the first time a direct comparison has been made between the cumulative hard X-ray spectral energy distribution of the local AGN population and the CXB spectrum, which demonstrated that the commonly accepted paradigm of the CXB being a superposition of AGN is grossly correct. Improved measurements of the cumulative spectral distribution and evolution of AGN by current and future X-ray and hard X-ray astronomy missions will make it possible to obtain tighter constraints on the cosmic history of black hole growth and the AGN unification paradigm.

Acknowledgments This work was supported by the DFG-Schwerpunktprogramme (SPP 1177). INTEGRAL is an ESA project funded by ESA member states (especially the PI countries: Denmark, France, Germany, Italy, Spain, Switzerland), Czech Republic and Poland, and with the participation of Russia and the USA. The research made use of the NASA/IPAC Extragalactic Database (operated by the Jet Propulsion Laboratory, California Institute of Technology) and the High Energy Astrophysics Science Archive Research Center Online Service (provided by the NASA/Goddard Space Flight Center).

References

Akylas, A., Georgantopoulos1, I., Georgakakis, A., Kitsionas, S., & Hatziminaoglou, E., 2006, A&A, 459, 693

Arnaud, K.A., 1996, Astronomical Data Analysis Software and Systems V, eds. Jacoby, G. & Barnes, J., ASP Conf. Series, 101, 17

Barger, A.J., Cowie, L.L., Mushotzky, R.F., et al., 2005, AJ, 129, 578

Bassani, L., Molina, M., Malizia, A., et al., 2006, ApJ, 636, L65

Beckmann, V., Soldi, S., Shrader, C.R., Gehrels, N., & Produit, N., 2006, ApJ, 652, 126
Bikmaev, I.F., Sunyaev, R.A., Revnivtsev, M.G., & Burenin, R.A., 2006, Astr. Lett., 32, 221
Brandt, W.N., & Hasinger, G., 2005, ARA&A, 43, 827
Churazov, E., Sunyaev, R., Revnivtsev, M., Sazonov, S., Molkov, S., Grebenev, S., et al., 2007, A&A, 467, 529
Elvis, M., Soltan, A., & Keel, W.C., 1984, ApJ, 283, 479
Gilli, R., Comastri, A., Hasinger, 2007, A&A, 463, 79
Gruber, D.E., Matteson, J.L., Peterson, L.E., & Jung, G.V., 1999, ApJ, 520, 124
Hecman, T., Kauffmann, G., Brinchmann, J., Charlot, S., Tremonti, C., & White, S. 2004, ApJ, 613, 109
Jourdain, E., Bassani, L., Buchet, L., et al., 1992, A&A, 256, L38
Krivonos, R., Revnivtsev, M., Lutovinov, A., Sazonov, S., Churazov, E., & Sunyaev, R., 2007, A&A (in press); arXiv:astro-ph/0701836
La Franca, F., Fiore, F., Comastri, A., et al., 2005, 635, 864
Landi, R., Masetti, N., Morelli, L., et al, 2007, ApJ (in press); arXiv:0706.3460
Markwardt, C.B., Tueller, J., Skinner, G.K., Gehrels, N., Barthelmy, S.D., & Mushotzky, R.F., 2005, ApJ, 633, L77
Masetti, N., Mason, E., Bassani, L., et al., 2006, A&A, 448, 547
Masetti, N., Morelli, L., Palazzi, E., et al., 2006, A&A, 459, 21
Masetti, N., Morelli, L., Cellone, S.A., et al., 2007, ATel 1033
Morelli, L., Masetti, N., Bassani, L., et al., 2006, ATel 785
Molina, M., Malizia, A., Bassani, L., et al., 2006, MNRAS, 371, 821
Perola, G.C., Matt, G., Cappi, M., Fiore, F., Guainazzi, M., Maraschi, L., et al., 2002, A&A, 389, 802
Revnivtsev, M., Sazonov, S., Jahoda, K., & Gilfanov, M., 2004, A&A, 418, 927
Revnivtsev, M., Sazonov, S., Churazov, E., & Trudolyubov, S., 2006, A&A, 448, L49
Reynolds, C.S., 1997, MNRAS, 286, 513
Sazonov, S., & Revnivtsev, M., 2004, A&A, 423, 469
Sazonov, S., Churazov, E., Revnivtsev, M., Vikhlinin, A., & Sunyaev, R., 2005, A&A, 444, L37
Sazonov, S., Revnivtsev, M., Krivonos, R., Churazov, E., & Sunyaev, 2007, A&A, 462, 57
Saunders, W., Sutherland, W.J., Maddox, S.J., et al., 2000, MNRAS, 317, 55
Setti G., & Woltjer L., 1989, A&A, 224, L21
Shakura, N.I., & Sunyaev, R.A., 1976, MNRAS, 175, 613
Shinozaki, K., Miyaji, T., Ishisaki, Y., Ueda, Y., & Ogasaka, Y., 2006, ApJ, 131, 2943
Tozzi, P., Gilli, R., Mainieri, V., et al., 2006, A&A, 451, 457
Treister, E., & Urry, M., 2006, ApJ, 652, L79
Tully, R.B. 1988, Nearby Galaxies Catalogue, Cambridge University Press
Turner, T.J., George, I.M., Nandra, K., & Mushotzky, R.F., 1997, ApJS, 113, 23
Ubertini, P., Lebrun, F., Di Cocco, G., et al., 2003, A&A, 411, L131
Ueda, Y., Akayama, M., Ohta, K., & Miyaji, T., 2003, ApJ, 598, 886
Ueda, Y., Eguchi, S., Terashima, Y., et al., 2007, ApJ, 664, L79
Winkler, C., Courvoisier, T.J.-L., Di Cocco, G., et al., 2003, A&A, 411, L1
Wright, E.L., Mather, J.C., Fixsen, D.J., et al., 1994, ApJ, 420, 450
Zdziarski, E.L., 1995, ApJ, 438, L63